scientific reports

OPEN

Semianalytical solution for the transient temperature in a scattering and absorbing slab consisting of three layers heated by a light source

Dominik Reitzle✉, Simeon Geiger, André Liemert & Alwin Kienle

We derived a semianalytical solution for the time-dependent temperature distribution in a three-layered laterally infinite scattering and absorbing slab illuminated by an obliquely incident collimated beam of light. The light propagation was modeled by the low-order P_1 and P_3 approximations to the radiative transfer equation with closed form expressions for eigenvalues and eigenvectors, yielding a quickly computable solution, while the heat conduction was modeled by the Fourier equation. The solution was compared to a numerical solution using a Monte Carlo simulation for the light propagation and an FEM method for the heat conduction. The results showed that using the P_3 solution for the light propagation offers a large advantage in accuracy with only a moderate increase in calculation time compared to the P_1 solution. Also, while the P_3 solution is not a very good approximation for the spatially resolved absorbance itself, its application as a source term for the heat conduction equation does yield a very good approximation for the time-dependent temperature.

Non-contact thermal property measurement methods are widely used because they avoid contact resistances and require little to no sample preparation[1]. While there is a large variety of detection principles, most techniques use optical heating in the visual and near-infrared range. Specifically in photothermal radiometry (PTR), the detection is based on recording the thermal emission using an IR sensor. In the recent past, PTR has e.g. been used to retrieve microhardness profiles in case hardened steel[2], detect partial curing in dental resins[3] or study drug diffusion in human skin[4]. For semi-transparent, non-scattering media, Ravi et al. studied the reconstruction of absorption profiles using modulated PTR[5], while Salazar et al. used the same method to simultaneously retrieve the absorption and thermal diffusivity profiles in semi-infinite media[6] and multi-layered slabs[7], utilizing analytical solutions of the heat conduction equation. Recently, Ren et al. extended this to temperature-dependent medium parameters for a 1D planar symmetric medium with coupled radiation and conduction using numerical solutions[8], but also specifically excluded scattering. Apart from parameter retrieval with PTR, the required forward solutions can also be used to predict temperature distributions and, especially in biomedical applications, thermal damage after laser irradiation[9]. Here, as in many other media, light scattering is a large effect and therefore must be accounted for in a model for optical heating. The radiative transfer equation (RTE) is generally considered a very accurate model for light propagation on mesoscopic and macroscopic scales for scattering and absorbing media[10]. But due to its complexity, the RTE is often replaced by the diffusion equation (DE)[11,12], which may be derived as an approximation to the RTE. Solutions to the DE are usually simple and can be computed quickly, but they are known to be inaccurate in many cases[13]. The P_N approximations to the RTE[14] on the other hand offer a much higher accuracy, but the computation time increases rapidly with the approximation order N. For low approximation orders N however, quickly computable closed form expressions can still be found[15]. While these low approximation order solutions can still exhibit large errors for the spatially resolved fluence or absorbance rate, their low spatial frequency components are already quite accurate. Using them as a source term for the heat conduction equation should therefore already produce highly accurate solutions for the medium temperature. The aim of this work therefore is to derive a semianalytical solution for the time-dependent temperature distribution in a three-layered scattering and absorbing medium heated by an incident beam of light, where the

Institut für Lasertechnologien in der Medizin und Meßtechnik an der Universität Ulm, Helmholtzstr. 12, 89081 Ulm, Germany. ✉email: dominik.reitzle@ilm-ulm.de

light propagation is modeled using low order P_N approximation to the RTE. Specifically, we use the expansion orders $N = 1$, which leads to a diffusion-like approximation, and $N = 3$, for which closed form expressions are available for the homogeneous solution, resulting in short computation times.

In "Solution of the RTE" section, we present our light propagation model using the P_N approximation to the RTE, including the used source and the optical boundary conditions for the three-layered medium. From this, we derive the source term for the heat conduction model, which is described in "Solution of the heat equation" section. Finally, in "Results and discussion" section, we compare the results of our solution to a purely numerical solution for a simple model of human skin.

Solution of the RTE

General solution. The steady-state radiative transport equation (RTE) governing the radiance $I(\mathbf{r}, \hat{\mathbf{s}})$ at position $\mathbf{r}$ and direction $\hat{\mathbf{s}}$ for a point source at $\mathbf{r} = \mathbf{0}$ radiating in direction $\hat{\mathbf{s}}_0$ is given by

$$\hat{\mathbf{s}} \cdot \nabla I(\mathbf{r}, \hat{\mathbf{s}}) + \mu_t I(\mathbf{r}, \hat{\mathbf{s}}) - \mu_s \int_{\mathbb{S}^2} I(\mathbf{r}, \hat{\mathbf{s}}') f(\hat{\mathbf{s}} \cdot \hat{\mathbf{s}}') \mathrm{d}^2 s' = \delta(\mathbf{r}) \delta(\hat{\mathbf{s}} - \hat{\mathbf{s}}_0) \tag{1}$$

with the phase function

$$f(\hat{\mathbf{s}} \cdot \hat{\mathbf{s}}') = \sum_{l=0}^{\infty} \frac{2l+1}{4\pi} f_l P_l(\hat{\mathbf{s}} \cdot \hat{\mathbf{s}}'), \tag{2}$$

where μ_a is the absorption coefficient, μ_s is the scattering coefficient, $\mu_t = \mu_a + \mu_s$ is the attenuation coefficient, f_l are the phase function moments and P_l the Legendre polynomials. In order to improve the accuracy of low order P_N approximations, we first approximate the phase function using the delta-M method[16,17] of order N as

$$f(\hat{\mathbf{s}} \cdot \hat{\mathbf{s}}') \approx \frac{f_{N+1}}{2\pi} \delta(1 - \hat{\mathbf{s}} \cdot \hat{\mathbf{s}}') + \sum_{l=0}^{N} \frac{2l+1}{4\pi} (f_l - f_{N+1}) P_l(\hat{\mathbf{s}} \cdot \hat{\mathbf{s}}'). \tag{3}$$

Next, we split a ballistic part off the radiance as $I = I_0 + I_d$. The ballistic part I_0 is then given by[18]

$$I_0(\mathbf{r}, \hat{\mathbf{s}}) = \frac{e^{-\tilde{\mu}_t r}}{r^2} \delta(\hat{\mathbf{r}} - \hat{\mathbf{s}}_0) \delta(\hat{\mathbf{s}} - \hat{\mathbf{s}}_0), \tag{4}$$

where the modified extinction coefficient becomes $\tilde{\mu}_t = \mu_a + (1 - f_{N+1})\mu_s$. The diffuse radiance I_d then satisfies the modified RTE

$$\hat{\mathbf{s}} \cdot \nabla I_d + \tilde{\mu}_t I_d - \mu_s \int_{\mathbb{S}^2} I_d \sum_{l=0}^{N} \frac{2l+1}{4\pi} (f_l - f_{N+1}) P_l(\hat{\mathbf{s}} \cdot \hat{\mathbf{s}}') \mathrm{d}^2 s' = S(\mathbf{r}, \hat{\mathbf{s}}, \hat{\mathbf{s}}_0), \tag{5}$$

with the new source term

$$S(\mathbf{r}, \hat{\mathbf{s}}, \hat{\mathbf{s}}_0) = \mu_s \frac{e^{-\tilde{\mu}_t r}}{r^2} \delta(\hat{\mathbf{r}} - \hat{\mathbf{s}}_0) \sum_{l=0}^{N} \frac{2l+1}{4\pi} (f_l - f_{N+1}) P_l(\hat{\mathbf{s}} \cdot \hat{\mathbf{s}}_0). \tag{6}$$

This new source corresponds to a line source in direction $\hat{\mathbf{s}}_0$ with exponentially decreasing fluence, radiating with the modified phase function rotated in beam direction. In the P_N method, the diffuse radiance is expanded in spherical harmonics Y_{lm} with expansion coefficients Ψ_{lm} as

$$I_d(\mathbf{r}, \hat{\mathbf{s}}) = \sum_{l=0}^{N} \sum_{m=-l}^{l} \Psi_{lm}(\mathbf{r}) Y_{lm}(\hat{\mathbf{s}}). \tag{7}$$

Using the transformed quantity

$$\tilde{\Psi}_{lm}(q, \phi_q, z) e^{-im\phi_q} = \int_0^{\infty} \int_0^{2\pi} \Psi_{lm}(\rho, \varphi, z) e^{-i\rho q \cos(\varphi - \phi_q)} \rho \mathrm{d}\rho \mathrm{d}\varphi, \tag{8}$$

the P_N equations are then given by[15]

$$\begin{aligned} &a_{l-1}^m \frac{\partial \tilde{\Psi}_{l-1,m}}{\partial z} + b_{l+1}^m \frac{\partial \tilde{\Psi}_{l+1,m}}{\partial z} + \tilde{\sigma}_l \tilde{\Psi}_{l,m} - \frac{iq}{2} \left(c_{l-1}^{m-1} \tilde{\Psi}_{l-1,m-1} - d_{l+1}^{m-1} \tilde{\Psi}_{l+1,m-1} \right) \\ &+ \frac{iq}{2} \left(c_{l-1}^{-m-1} \tilde{\Psi}_{l-1,m+1} - d_{l+1}^{-m-1} \tilde{\Psi}_{l+1,m+1} \right) = E_{lm}(q, \phi_q, z), \end{aligned} \tag{9}$$

for $0 \le m \le N$ and $m \le l \le N$ with the condition

$$\tilde{\Psi}_{l,-m} = (-1)^m \tilde{\Psi}_{l,m}, \tag{10}$$

where the right hand side E_{lm} must be determined from the source term (see Eq. (15)). The coefficients are given by[15]

$$\tilde{\sigma}_l = \tilde{\mu}_t - (f_l - f_{N+1})\mu_s = \mu_t - f_l\mu_s = \sigma_l \tag{11}$$

and

$$\begin{aligned} a_l^m &= \sqrt{\frac{(l-m+1)(l+m+1)}{(2l+1)(2l+3)}}, \quad b_l^m = \sqrt{\frac{(l-m)(l+m)}{(2l-1)(2l+1)}}, \\ c_l^m &= \sqrt{\frac{(l+m+1)(l+m+2)}{(2l+1)(2l+3)}}, \quad d_l^m = \sqrt{\frac{(l-m)(l-m-1)}{(2l-1)(2l+1)}}. \end{aligned} \tag{12}$$

Note that the rotation $e^{-im\phi_q}$ in Eq. (8) makes the left hand side of the system (9) independent of ϕ_q, allowing a much more efficient numerical evaluation. The σ_l in Eq. (11) are the coefficients that follow directly from applying the P_N method to Eq. (1) without the delta-M method and the ballistic part separation[14]. It is therefore evident that the homogeneous solutions of Eqs. (1) and (5) are identical. These solutions can for example be found using the method of rotated reference frames, which was studied intensively over the last few years. The solution for the diffuse radiance then has the form[14]

$$\begin{aligned} I_d(q,\phi_q,z,\theta,\varphi) = \sum_{l=0}^{N}\sum_{m=-l}^{l}\Bigg[&\sum_i C_i(q,\phi_q)e^{-\sqrt{q^2+\frac{1}{\xi_i^2}}z}\Lambda_{lm}^i(q) \\ &+\sum_i C_i'(q,\phi_q)e^{\sqrt{q^2+\frac{1}{\xi_i^2}}z}(-1)^l\Lambda_{lm}^i(q) + \tilde{\Psi}_{lm}^{(p)}(q,\phi_q,z)\Bigg]Y_{lm}(\theta,\varphi-\phi_q). \end{aligned} \tag{13}$$

Here, C_i and C_i' are unknown coefficients determined by the boundary conditions, $\sqrt{q^2+\frac{1}{\xi_i^2}} =: \zeta_i(q)$ are the positive eigenvalues and $\Lambda_{lm}^i(q)$ the corresponding eigenvector components. We refer the reader to previous publications[14,15,19–21] for details on this method.

For the particular solution $\tilde{\Psi}_{lm}^{(p)}(q,\phi_q,z)$ with the source term (6), we first calculate its spherical harmonics decomposition

$$\epsilon_{lm}(\mathbf{r}) = \int_{\mathbb{S}^2} S(\mathbf{r},\hat{\mathbf{s}},\hat{\mathbf{s}}_0)Y_{lm}^*(\hat{\mathbf{s}})\mathrm{d}^2s = \mu_s\frac{e^{-\tilde{\mu}_t r}}{r^2}\delta(\hat{\mathbf{r}}-\hat{\mathbf{s}}_0)(f_l-f_{N+1})Y_{lm}^*(\hat{\mathbf{s}}_0). \tag{14}$$

Applying a 2D Fourier transform, setting $\hat{\mathbf{s}}_0 = (\theta_0, 0)$ in spherical coordinates and making use of condition (10), we obtain the desired moments

$$E_{lm}(q,\phi_q,z) = \frac{\mu_s}{|\mu_0|}\Theta(\frac{z}{\mu_0})e^{-\frac{\tilde{\mu}_t}{\mu_0}z}e^{-iqz\tan(\theta_0)\cos(\phi_q)}(f_l-f_{N+1})\Re\{Y_{lm}(\theta_0,\phi_q)\}, \tag{15}$$

with $\mu_0 = \cos(\theta_0)$. Introducing the abbreviation[22]

$$\mu_c = \frac{\tilde{\mu}_t}{\mu_0} + iq\tan(\theta_0)\cos(\phi_q), \tag{16}$$

the similarity ansatz $\tilde{\Psi}_{lm}^{(p)} = \chi_{lm}e^{-\mu_c z}$ can be used to solve the system (9) with the source moments (15), resulting in the system of equations for $z \geq 0$ and $1 \geq \mu_0 > 0$

$$\begin{aligned} -\mu_c\left(a_{l-1}^m\chi_{l-1,m} + b_{l+1}^m\chi_{l+1,m}\right) + \sigma_l\chi_{l,m} - \frac{iq}{2}\left(c_{l-1}^{m-1}\chi_{l-1,m-1} - d_{l+1}^{m-1}\chi_{l+1,m-1}\right) \\ +\frac{iq}{2}\left(c_{l-1}^{-m-1}\chi_{l-1,m+1} - d_{l+1}^{-m-1}\chi_{l+1,m+1}\right) = \frac{\mu_s}{\mu_0}(f_l-f_{N+1})\Re\{Y_{lm}(\theta_0,\phi_q)\}. \end{aligned} \tag{17}$$

In many cases, only the fluence rate $\Phi(q,\phi_q,z) = \int_{\mathbb{S}^2} I(q,\phi_q,z,\hat{\mathbf{s}})\mathrm{d}^2s$ is required instead of the radiance from Eqs. (4) and (13). Using the same set of polar coordinates for the ballistic part, the fluence rate is found to be

$$\Phi_0(q,\phi_q,z) = \frac{1}{|\mu_0|}\Theta\left(\frac{z}{\mu_0}\right)e^{-\mu_c z}, \tag{18}$$

$$\Phi_d(q,\phi_q,z) = \sqrt{4\pi}\sum_i\left[C_i(q,\phi_q)e^{-\zeta_i(q)z} + C_i'(q,\phi_q)e^{\zeta_i(q)z}\right]\Lambda_{00}^i(q) + \sqrt{4\pi}\,\chi_{00}(q,\phi_q)e^{-\mu_c z}. \tag{19}$$

RTE boundary conditions for a three-layered slab. Our goal here is to construct a solution for a stack of three laterally infinite layers, where for simplicity all layers share the same refractive index. The refractive index outside the stack may, however, be different from the one inside so that Fresnel reflection at the top and bottom surfaces must be accounted for in the boundary conditions. Figure 1 illustrates this problem geometry schematically.

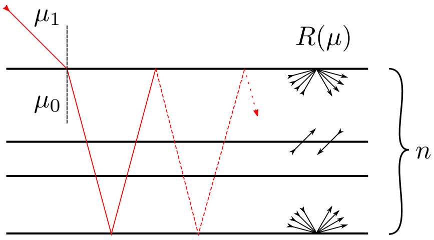

Figure 1. Schematic of the problem geometry. A stack of three laterally infinite layers is illuminated by a collimated beam with angle cosines of μ_1 and μ_0 outside and inside of the stack, respectively. On the top and bottom surface, Fresnel reflections must be accounted for, while the radiance is continuous at the layer interfaces.

To that end, we first rescale the coefficients C_i and C_i' from equation (13) for each layer $n \in \{1, 2, 3\}$ with thickness $L^{(n)}$ and take the extinction and shift $D(n)$ of the incident light by the layers above into account, resulting in

$$\begin{aligned} I_d^{(n)}(q, \phi_q, z, \theta, \varphi) = \sum_{l=0}^{N} \sum_{m=-l}^{l} \Bigg[\sum_i C_i^{(n)}(q, \phi_q) e^{-\zeta_i^{(n)}(q)(z-\lambda^{(n)})} \Lambda_{lm}^{i,(n)}(q) \\ + \sum_i C_i'^{(n)}(q, \phi_q) e^{\zeta_i^{(n)}(q)(z-\lambda^{(n)}-L^{(n)})} (-1)^l \Lambda_{lm}^{i,(n)}(q) \\ + \chi_{lm}^{(n)}(q, \phi_q, z) e^{-\mu_c^{(n)}(z-\lambda^{(n)})} D(n) \Bigg] Y_{lm}(\theta, \varphi - \phi_q), \end{aligned} \tag{20}$$

where we defined

$$\lambda^{(n)} = \sum_{k=1}^{n-1} L^{(k)}, \tag{21}$$

and

$$D(n) = \prod_{k=1}^{n-1} e^{-\mu_c^{(k)} L^{(k)}}. \tag{22}$$

Using $\mu = \cos(\theta)$ and $\mu > 0$, the boundary conditions are given by[13]

$$I^{(1)}(z = 0, \mu, \varphi) = R(\mu) I^{(1)}(z = 0, -\mu, \varphi), \tag{23}$$

$$I^{(3)}(z = \lambda^{(4)}, -\mu, \varphi) = R(\mu) I^{(3)}(z = \lambda^{(4)}, \mu, \varphi), \tag{24}$$

$$I^{(n)}(z = \lambda^{(n+1)}, \mu, \varphi) = I^{(n+1)}(z = \lambda^{(n+1)}, \mu, \varphi), \quad n = \{1, 2\}, \tag{25}$$

$$I^{(n)}(z = \lambda^{(n+1)}, -\mu, \varphi) = I^{(n+1)}(z = \lambda^{(n+1)}, -\mu, \varphi), \quad n = \{1, 2\}, \tag{26}$$

where $R(\mu)$ is the Fresnel reflection coefficient for the top and bottom surfaces[23]. Multiplying all conditions with $Y^*_{l'm'}(\mu, \varphi)$ and integrating over the half-space $\mu > 0$ then yields the generalized Marshak boundary conditions[14,22,24]. Suppressing the arguments from Eq. (20), we get from Eq. (23) for the top surface

$$\sum_l R_{l'l}^{m'} \left(\sum_i C_i^{(1)} \Lambda_{lm'}^{i,(1)} + \sum_i C_i'^{(1)} e^{-\zeta_i^{(1)} L^{(1)}} (-1)^l \Lambda_{lm'}^{i,(1)} \right) = -\sum_l R_{l'l}^{m'} \chi_{lm'}^{(3)}, \tag{27}$$

from Eq. (24) for the bottom surface

$$\sum_l R_{l'l}^{m'} \left(\sum_i C_i^{(3)} e^{-\zeta_i^{(3)} L^{(3)}} (-1)^l \Lambda_{lm'}^{i,(3)} + \sum_i C_i'^{(3)} \Lambda_{lm'}^{i,(3)} \right) = -\sum_l R_{l'l}^{m'} (-1)^l D(4) \chi_{lm'}^{(3)}, \tag{28}$$

and from Eqs. (25) and (26) with $n = \{1, 2\}$ for the interfaces between the layers

$$\sum_l T_{l'l}^{m'}\left(\sum_i C_i^{(n)} e^{-\zeta_i^{(n)}L^{(n)}}\Lambda_{lm'}^{i,(n)} + \sum_i C_i'^{(n)}(-1)^l\Lambda_{lm'}^{i,(n)} - \sum_i C_i^{(n+1)}\Lambda_{lm'}^{i,(n+1)}\right.$$
$$\left. - \sum_i C_i'^{(n+1)} e^{-\zeta_i^{(n+1)}L^{(n+1)}}(-1)^l\Lambda_{lm'}^{i,(n+1)}\right) = \sum_l T_{l'l}^{m'} D(n+1)\left(\chi_{lm'}^{(n+1)} - \chi_{lm'}^{(n)}\right), \tag{29}$$

and

$$\sum_l T_{l'l}^{m'}(-1)^l\left(\sum_i C_i^{(n)} e^{-\zeta_i^{(n)}L^{(n)}}\Lambda_{lm'}^{i,(n)} + \sum_i C_i'^{(n)}(-1)^l\Lambda_{lm'}^{i,(n)} - \sum_i C_i^{(n+1)}\Lambda_{lm'}^{i,(n+1)}\right.$$
$$\left. - \sum_i C_i'^{(n+1)} e^{-\zeta_i^{(n+1)}L^{(n+1)}}(-1)^l\Lambda_{lm'}^{i,(n+1)}\right) = \sum_l T_{l'l}^{m'}(-1)^l D(n+1)\left(\chi_{lm'}^{(n+1)} - \chi_{lm'}^{(n)}\right). \tag{30}$$

Here, the coefficients $R_{ll'}^{m'}$ for the Fresnel reflection at the top and bottom surfaces are given by[14,21]

$$R_{ll'}^{m'} = \sqrt{\frac{(2l+1)(2l'+1)(l-m')!(l'-m')!}{(l+m')!(l'+m')!}} \times \int_0^1 \left[1-(-1)^{l+m'}R(\mu)\right] P_l^{m'}(\mu)P_{l'}^{m'}(\mu)\mathrm{d}\mu, \tag{31}$$

while the transmission coefficients $T_{ll'}^{m'}$ for the boundaries between layers are

$$T_{ll'}^{m'} = \sqrt{\frac{(2l+1)(2l'+1)(l-m')!(l'-m')!}{(l+m')!(l'+m')!}} \times \int_0^1 P_l^{m'}(\mu)P_{l'}^{m'}(\mu)\mathrm{d}\mu. \tag{32}$$

Following the standard prescription for the generalized Marshak boundary conditions[14] by picking for each $l' = 1,\ldots,N$ the Eqs. (27)–(30) with $m' = l'-1, l'-3, \ldots$ results in a system of equations that determines all unknown coefficients $C_i^{(n)}$ and $C_i'^{(n)}$, completing the solution for the P_N approximation to the RTE. In all of the above, a single source with unit strength just below the upper boundary was assumed. To model an incident collimated beam from outside the medium, we have to take the Fresnel reflection outside the medium as well as internal reflections of the unscattered light into account. If $R_d(\mu_1)$ is the reflection coefficient outside the medium and $R_0 = R(\mu_0)$ the reflection coefficient inside the medium, where μ_1 and μ_0 are connected by Snell's law, the sources due to multiple internal reflections can be reduced to two sources with strengths S_o and S_u for the top and bottom surface, respectively, with

$$S_o = (1-R_d)\sum_{n=0}^{\infty}\left(R_0^2 D(4)^2\right)^n = \frac{1-R_d}{1-R_0^2 D(4)^2}, \tag{33}$$

$$S_u = R_0 D(4) S_o. \tag{34}$$

In many cases, $R_0 D(4)$ is very small and the lower source may be neglected. If however the medium is optically thin enough for the lower source to matter, the coefficients $C_i^{(n)}$ and $C_i'^{(n)}$ must be recalculated with reversed layer order for a complete solution.

Solution of the heat equation

We assume that the heat transport inside the medium is governed by the differential equation

$$\rho^{(n)} c_p^{(n)} \frac{\partial T(\mathbf{r},t)}{\partial t} - k^{(n)}\Delta T(\mathbf{r},t) = \delta_{nm} Q_s(x,y)\delta(z-z_0)Q_t(t)\Theta(t) \tag{35}$$

for the temperature $T(\mathbf{r},t)$, where ρ is the density, c_p the heat capacity and k the isotropic thermal conductivity. n is the layer number and m the layer containing a source sheet at depth z_0 with spatial profile $Q_s(x,y)$ and time dependence $Q_t(t)\Theta(t)$. For the heat equation (35) to be valid, the spectral components of $Q_t(t)$ must be restricted to frequencies well below 1 GHz[25]. This allows using the steady-state RTE absorbance for the spatial source profile. Also, the layers should be at least several micrometers thick. Applying the same 2D-Fourier transform we used for the RTE and a Laplace transform with respect to time to (35) using $T = 0$ everywhere as initial condition, we get with the Laplace variable s

$$\left(\frac{\partial^2}{\partial z^2} - (\alpha^{(n)})^2\right)\tilde{T}^{(n)}(s,q,\phi_q,z) = -\delta_{nm}\frac{1}{k^{(n)}}\tilde{Q}_s(q,\phi_q)\tilde{Q}_t(s)\delta(z-z_0), \tag{36}$$

with

$$\alpha^{(n)} = \sqrt{\frac{\rho^{(n)} c_p^{(n)}}{k^{(n)}} s + q^2}, \tag{37}$$

where the tilde marks transformed quantities. We note that in our previous work[26], we derived a more general solution of the heat conduction equation for N layers with anisotropic thermal conductivities. The solution we require here, therefore, arises as a special case and is given by

$$\tilde{T}_m^{(n)}(s,q,\phi_q,z,z_0) = A_m^{(n)} e^{\alpha^{(n)}(z-\lambda^{(n)}-L^{(n)})} + B_m^{(n)} e^{-\alpha^{(n)}(z-\lambda^{(n)})} + \delta_{nm}\tilde{P}^{(m)}(s,q,\phi_q,z,z_0), \tag{38}$$

$$\tilde{P}^{(m)}(s,q,\phi_q,z,z_0) = \frac{\tilde{Q}_s(q,\phi_q)\tilde{Q}_t(s)}{2k^{(m)}\alpha^{(m)}} e^{-\alpha^{(m)}|z-z_0|}. \tag{39}$$

The coefficients $A_m^{(n)}$ and $B_m^{(n)}$ are determined by the boundary conditions for the heat equation, where we used Robin-type convective boundary conditions for the upper and lower boundaries and the perfect thermal contact between layers, resulting in a system of equations for each m. For the special case of three layers, we arrive at

$$\mathbf{M}\cdot\begin{pmatrix} A_m^{(1)} \\ B_m^{(1)} \\ A_m^{(2)} \\ B_m^{(2)} \\ A_m^{(3)} \\ B_m^{(3)} \end{pmatrix} = \begin{pmatrix} -\delta_{m1}\frac{1}{k^{(1)}} f_2^{(0)}\left(1-\frac{h_1}{k^{(1)}\alpha^{(1)}}\right) \\ -\delta_{m1}\frac{1}{k^{(1)}\alpha^{(1)}} f_1^{(1)} + \delta_{m2}\frac{1}{k^{(2)}\alpha^{(2)}} f_2^{(1)} \\ \delta_{m1} f_1^{(1)} + \delta_{m2} f_2^{(1)} \\ -\delta_{m2}\frac{1}{k^{(2)}\alpha^{(2)}} f_1^{(2)} + \delta_{m3}\frac{1}{k^{(3)}\alpha^{(3)}} f_2^{(2)} \\ \delta_{m2} f_1^{(2)} + \delta_{m3} f_2^{(2)} \\ \delta_{m3}\frac{1}{k^{(3)}} f_1^{(3)}\left(1-\frac{h_2}{k^{(3)}\alpha^{(3)}}\right) \end{pmatrix}, \tag{40}$$

with

$$f_1^{(m)} = \frac{\tilde{Q}_s(q,\phi_q)\tilde{Q}_t(s)}{2} e^{-\alpha^{(m)}(\lambda^{(m+1)}-z_0)}, \tag{41}$$

$$f_2^{(m)} = \frac{\tilde{Q}_s(q,\phi_q)\tilde{Q}_t(s)}{2} e^{-\alpha^{(m)}(z_0-\lambda^{(m+1)})}. \tag{42}$$

The matrix $\mathbf{M}$ is given in[26] and in Appendix A. In[26], we gave closed form expressions for the 6 coefficients $A_1^{(n)}$ and $B_1^{(n)}$ for a three-layered system and sources in the first layer. Since in our case there are sources in all layers, we also need the expressions for the remaining 12 coefficients. For sources in the third layer, they follow immediately from the coefficients for sources in the first layer with reversed layer properties. The coefficients $A_2^{(n)}$ and $B_2^{(n)}$ for sources in the second layer, however, must be calculated separately and are given in Appendix A. The spatial source distribution $\tilde{Q}_s(q,\phi_q)$ at depth z_0 is now given by the corresponding RTE absorbance

$$\tilde{Q}_s(q,\phi_q,z_0) = \mu_a^{(m)}\Phi^{(m)}(q,\phi_q,z_0), \tag{43}$$

with the fluence

$$\begin{aligned}\Phi^{(m)}(q,\phi_q,z_0) = \sqrt{4\pi}\sum_i \Lambda_{00}^{i,(m)}(q)\left[C_i^{(m)}(q,\phi_q)e^{-\zeta_i^{(m)}(q)(z_0-\lambda^{(m)})} + C_i'^{(m)}(q,\phi_q)e^{\zeta_i^{(m)}(q)(z_0-\lambda^{(m)}-L^{(m)})}\right] \\ + \left(\sqrt{4\pi}\,\chi_{00}^{(m)}(q,\phi_q) + \frac{1}{|\mu_0|}\right)D(m)e^{-\mu_c^{(m)}(z-\lambda^{(m)})}.\end{aligned} \tag{44}$$

With the contributions from all depths known, we can then calculate the complete solution as

$$\tilde{T}^{(n)}(s,q,\phi_q,z) = \sum_m \int_{\lambda^{(m)}}^{\lambda^{(m+1)}} \tilde{T}_m^{(n)}(s,q,\phi_q,z,z_0)\mathrm{d}z_0. \tag{45}$$

Looking at Eqs. (38) and (39), the integral in Eq. (45) for a fixed m only acts on the coefficients $f_1^{(m)}$ and $f_2^{(m-1)}$ and on the particular solution. We can, therefore, solve the integrals and obtain a closed form solution by replacing $f_1^{(m)}$ and $f_2^{(m-1)}$ in the solution of (40) with $\bar{f}_1^{(m)}$ and $\bar{f}_2^{(m-1)}$ as

$$\begin{aligned}\bar{f}_1^{(m)} = \frac{\mu_a^{(m)}\tilde{Q}_t(s)}{2}\Bigg\{\sqrt{4\pi}\sum_i \Lambda_{00}^{i,(m)}\left[C_i^{(m)}\frac{e^{-\alpha^{(m)}L^{(m)}} - e^{-\zeta_i^{(m)}L^{(m)}}}{\zeta_i^{(m)}-\alpha^{(m)}} + C_i'^{(m)}\frac{1-e^{-(\alpha^{(m)}+\zeta_i^{(m)})L^{(m)}}}{\zeta_i^{(m)}+\alpha^{(m)}}\right] \\ + \left(\sqrt{4\pi}\,\chi_{00}^{(m)} + \frac{1}{\mu_0}\right)D(m)\frac{e^{-\mu_c^{(m)}L^{(m)}} - e^{-\alpha^{(m)}L^{(m)}}}{\alpha^{(m)}-\mu_c^{(m)}}\Bigg\},\end{aligned} \tag{46}$$

and

	$\rho\,(\mathrm{kg\,m^{-3}})$	$c_p\,(\mathrm{J\,kg^{-1}\,K^{-1}})$	$k\,(\mathrm{W\,m^{-1}\,K^{-1}})$	l (mm)
1	1100	3000	0.25	1
2	900	3000	0.2	2
3	1100	3500	0.5	10

Table 1. Thermal parameters of the considered medium.

	$\mu_s'\,(\mathrm{mm^{-1}})$	$\mu_a\,(\mathrm{mm^{-1}})$	g	n_i
1	2.0	0.02	0.8	1.4
2	1.0	0.003	0.8	1.4
3	0.5	0.04	0.8	1.4

Table 2. Optical parameters of the considered medium. For the phase function, the Henyey–Greenstein function is used. The refractive index n_i must be identical for all layers, while the refractive index outside the medium is set to 1.0.

$$\begin{aligned}\bar{f}_2^{(m-1)} = \frac{\mu_a^{(m)}\tilde{Q}_t(s)}{2}\Bigg\{\sqrt{4\pi}\sum_i \Lambda_{00}^{i,(m)}\left[C_i^{(m)}\frac{1-e^{-(\alpha^{(m)}+\zeta_i^{(m)})L^{(m)}}}{\zeta_i^{(m)}+\alpha^{(m)}} + C_i'^{(m)}\frac{e^{-\alpha^{(m)}L^{(m)}}-e^{-\zeta_i^{(m)}L^{(m)}}}{\zeta_i^{(m)}-\alpha^{(m)}}\right]\\ +\left(\sqrt{4\pi}\,\chi_{00}^{(m)}+\frac{1}{\mu_0}\right)D(m)\frac{1-e^{-(\alpha^{(m)}+\mu_c^{(m)})L^{(m)}}}{\alpha^{(m)}+\mu_c^{(m)}}\Bigg\},\end{aligned} \tag{47}$$

and replacing the particular solution (39) with $\bar{P}^{(m)}(s,q,\phi_q,z)$ for $\lambda^{(m)} \le z \le \lambda^{(m+1)}$ as

$$\begin{aligned}\bar{P}^{(m)}(s,q,\phi_q,z) = \frac{\mu_a^{(m)}\tilde{Q}_t(s)}{2k^{(m)}\alpha^{(m)}}\Bigg\{\sqrt{4\pi}\sum_i \frac{\Lambda_{00}^{i,(m)}}{(\alpha^{(m)})^2-(\zeta_i^{(m)})^2}\\ \times\Big[C_i^{(m)}\Big(2\alpha^{(m)}e^{-\zeta_i^{(m)}(z-\lambda^{(m)})}+(\zeta_i^{(m)}-\alpha^{(m)})e^{-\zeta_i^{(m)}L^{(m)}}e^{-\alpha^{(m)}(\lambda^{(m+1)}-z)}\\ -(\zeta_i^{(m)}+\alpha^{(m)})e^{-\alpha^{(m)}(z-\lambda^{(m)})}\Big)+C_i'^{(m)}\Big(2\alpha^{(m)}e^{-\zeta_i^{(m)}(\lambda^{(m+1)}-z)}\\ +(\zeta_i^{(m)}-\alpha^{(m)})e^{-\zeta_i^{(m)}L^{(m)}}e^{-\alpha^{(m)}(z-\lambda^{(m)})}-(\zeta_i^{(m)}+\alpha^{(m)})e^{-\alpha^{(m)}(\lambda^{(m+1)}-z)}\Big)\Big]\\ +\left(\sqrt{4\pi}\,\chi_{00}^{(m)}+\frac{1}{\mu_0}\right)\frac{D(m)}{(\alpha^{(m)})^2-(\mu_c^{(m)})^2}\Big[2\alpha^{(m)}e^{-\mu_c^{(m)}(z-\lambda^{(m)})}\\ +(\mu_c^{(m)}-\alpha^{(m)})e^{-\mu_c^{(m)}L^{(m)}}e^{-\alpha^{(m)}(\lambda^{(m+1)}-z)}-(\mu_c^{(m)}+\alpha^{(m)})e^{-\alpha^{(m)}(z-\lambda^{(m)})}\Big]\Bigg\}.\end{aligned} \tag{48}$$

Results and discussion

In this section, the obtained solution is tested and validated against a purely numerical solution. As an exemplary system, we choose a three-layered generic model of human tissue in the near-infrared range[27,28]. The three layers represent skin, subcutaneous fat and muscle tissue, respectively. The thermal parameters of the model are listed in Table 1 and the optical parameters in Table 2. For all layers, we assume a refractive index of $n_i = 1.4$ with $n_o = 1.0$ outside the medium and the Henyey–Greenstein phase function with $g = 0.8$ using the moments $f_l = g^l$. For the upper boundary, we use a heat transfer coefficient of $h_1 = 100\,\mathrm{W\,m^{-2}\,K^{-1}}$ with an ambient temperature of $T_a = 0$ equal to the initial medium temperature and assume an adiabatic lower boundary with $h_2 = 0$.

As an input beam, we use a Gaussian beam with beam radius $r_w = 1$ mm hitting the top surface with an angle outside the medium of $\mu_1 = \cos(\theta_1)$, centered at the origin. We use $\theta_1 = 0°$ and $\theta_1 = 60°$ as incidence angles. Taking the distortion of the beam profile due to the oblique incidence into account, the input beam profile is then given by[22]

$$f(x,y) = \frac{2\mu_1}{\pi r_w^2}\exp\left\{-2\frac{\mu_1^2x^2+y^2}{r_w^2}\right\}. \tag{49}$$

Applying a 2D Fourier transform to (49) again yields

$$\tilde{F}(q,\phi_q) = \exp\left\{-\frac{1}{8}r_w^2q^2\left(\sin^2(\phi_q)+\frac{1}{\mu_1^2}\cos^2(\phi_q)\right)\right\}. \tag{50}$$

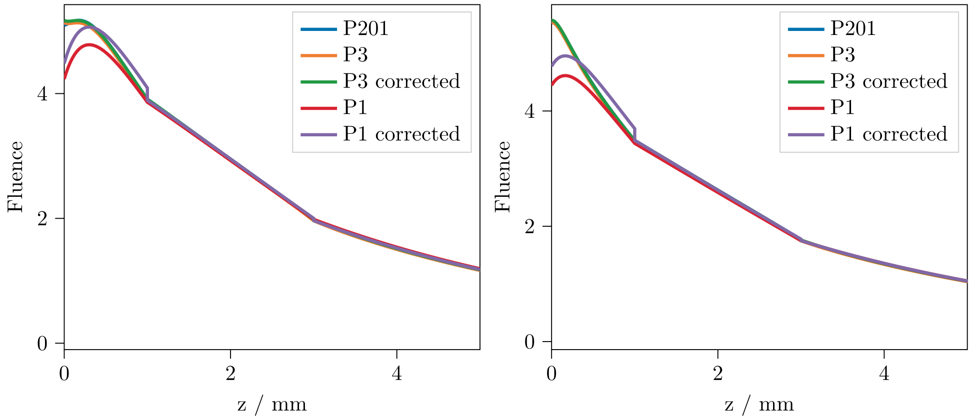

(a) $\theta_1 = 0°$ (b) $\theta_1 = 60°$

Figure 2. Depth-resolved fluence rate for the three-layered system, integrated over x and y. The P_{201} solution can be regarded as practically exact. For the corrected solutions, the total absorbance per layer was matched to the P_{201} solution.

		Layer 1	Layer 2	Layer 3
*P*1	0°	5.925%	0.7962%	−1.035%
	60°	7.428%	1.534%	0.0275%
*P*3	0°	0.7325%	0.7978%	0.8433%
	60°	0.7000%	0.8089%	0.8538%

Table 3. Total absorbance error for each layer of the P_1 and P_3 approximations relative to a P_{201} approximation that may be regarded as an exact solution.

The lower source strength from Eq. (34) depends on the approximation order and on the angle of incidence, but even for normal incidence with the P_1 approximation, it is nine orders of magnitude weaker than the upper source. Therefore, we can safely neglect the lower source in all calculations. As approximation orders, we consider only the P_1 and P_3 approximations, because for these, there are closed form expressions available for the eigenvalues and eigenvectors. For the P_3, we use the expressions given by Liemert et al.[15], while the P_1 expressions are given in Appendix B. Although theoretically possible up to P_7, no higher order closed form expressions are available to the authors' knowledge. Computing the eigenvalues and eigenvectors numerically is possible for higher orders, but computationally quite expensive. Also, the solution would become more and more unstable for high values of q, which would render the numerical inverse Fourier transform extremely tricky. To obtain a numerical solution to compare to, we use a two step process. First, the light propagation is calculated using a custom GPU-accelerated Monte Carlo solver, recording the spatially resolved fluence rate inside the medium. Then, we use the COMSOL Multiphysics software[29] to interpolate the resulting absorbance from the Monte Carlo simulation and calculate the time-dependent temperature rise.

Since we expect the P_N approximation to be the main source of error in the final results, we first look at the predicted fluence rate. Figure 2 contains the depth-resolved total fluence rate calculated in P_1 and P_3 approximation, integrated over x and y. Here, we do not yet have to resort to Monte Carlo methods to obtain a correct reference, since for planar symmetry or $q = 0$, the P_N equations can be solved efficiently for high orders N. Integrating the depth resolved total fluence rate over a layer and multiplying by the respective μ_a yields the total absorbance inside that layer. As the dependence on z of the fluence rate is very simple (compare Eqs. (18) and (19)), this integration can be done analytically and these total absorbances per layer can, therefore, be calculated with little computational effort. Table 3 contains the errors of the total absorbances per layer for the P_1 and P_3 approximations relative to the practically exact P_{201}. It can be seen that the P_3 is clearly superior to the simpler P_1 approximation. Especially in the vicinity of the light source near the upper boundary, the P_1 introduces large errors. However, the P_3 still underestimates the total fluence and therefore the total heat source strength per layer by $0.7 - 0.9\%$. Being able to quickly quantify these errors, in addition, enables us to correct them. This results in a weighting factor for the heat source strength in each layer, making sure that the total source strength in each layer, and consequently also in the whole medium, is correct. The corresponding fluence rates are also shown in Fig. 2.

We implemented our solution in Python. The implementation includes the planar symmetric P_N approximation solution, the 3D P_1 and P_3 approximation solutions, the solution of the heat equation with the P_1 and

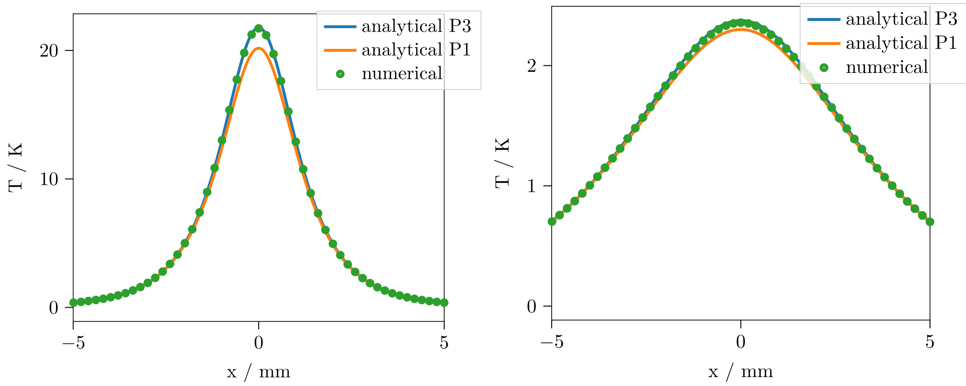

(a) $z = 0\,\mathrm{mm}$ (b) $z = 4\,\mathrm{mm}$

Figure 3. Temperature after $t = 15$ s with normal incidence $\theta_1 = 0°$ along the line $y = 0$ for two different depths. The P_3 approximation shows a good agreement with the numerical reference solution, while the P_1 exhibits a considerable error.

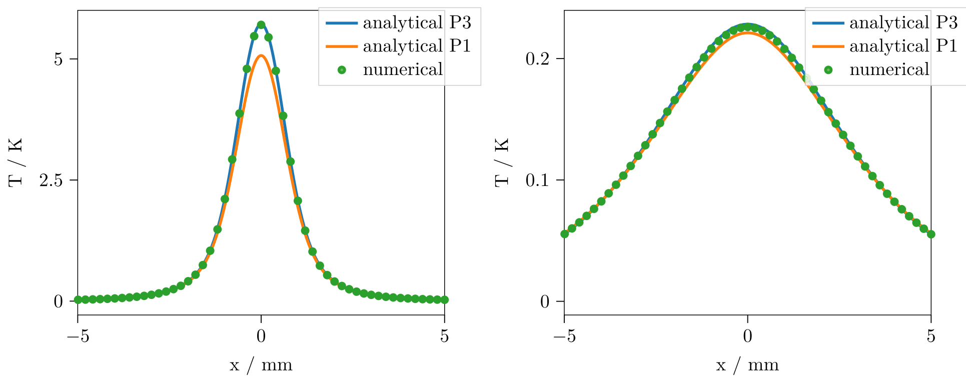

(a) $z = 0\,\mathrm{mm}$ (b) $z = 4\,\mathrm{mm}$

Figure 4. Temperature after $t = 1$ s with normal incidence $\theta_1 = 0°$ along the line $y = 0$ for two different depths. The results are slightly less accurate for short times, but the P_3 approximation still agrees well with the numerical reference solution.

P_3 absorbance sources and the required numerical transform algorithms and is freely available together with the reference results of the numerical calculations[30]. The transform algorithms are basically the same that were used in a previous work[26]. For the comparison, we calculate the results along the line $y = 0$ mm at two depths $z = 0$ mm and $z = 4$ mm, $t = 1$ s and $t = 15$ s after the source was switched on. Figures 3 and 4 show the results for normal incidence, while the results for an incident angle of $\theta_1 = 60°$ are shown in Figs. 5 and 6. For each curve, 400 points were calculated. The performance depends, of course, on the efficiency of the numerical transforms and on the required accuracy. For the present calculations, we used 39 points for the inverse Laplace transform and 240×80 points for the inverse 2D Fourier transform, which resulted in a computation time of 3.4 s for the P_3 approximation and 2.7 s for the P_1 approximation per curve on a standard desktop PC. For the numerical solution, the Monte Carlo simulation took 16 min and the subsequent finite element solution took 44 min to complete with reasonable accuracy. As can be seen, the P_3 solution agrees quite well with the numerical result, while the P_1 predictably shows larger errors up to 7%. For short times, the errors are slightly larger for all cases. This is to be expected, since the errors in the P_N absorbance are mostly contained in the high spatial frequency components. These are most prominent in the temperature solution for short times and then decrease due to the effects of heat conduction. To confirm that the remaining error of the P_3 approximation is indeed due to a slight misprediction of the heat source geometry instead of the interpolation or the finite element calculation, we repeated the numerical simulation with absorbance values computed from the P_3 approximation instead of the Monte Carlo simulation. For this comparison, we observed a practically exact agreement of the solutions.

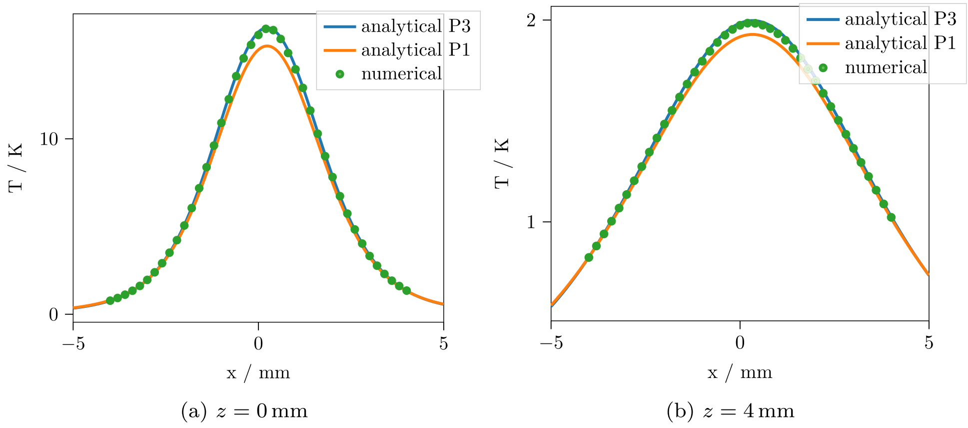

Figure 5. Temperature after $t = 15$ s with an incidence angle of $\theta_1 = 60°$ along the line $y = 0$ for two different depths. While the P_3 is still clearly superior to the P_1 approximation, neither of the approximations deteriorates much with oblique incidence.

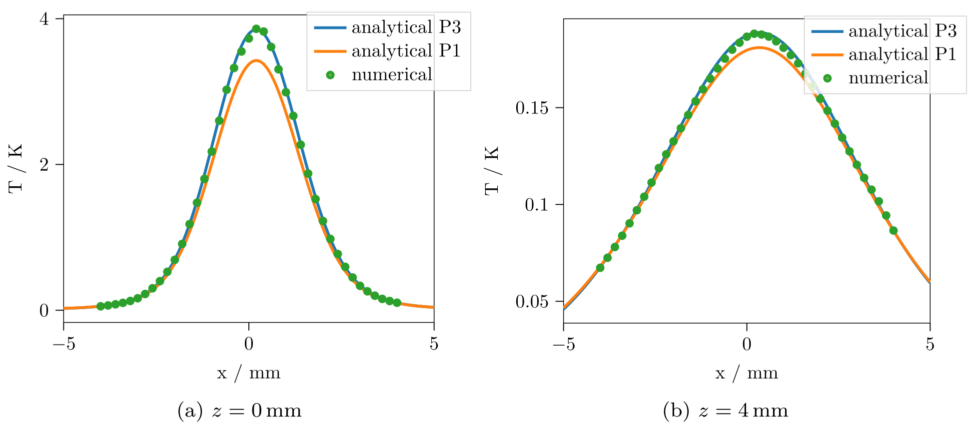

Figure 6. Temperature after $t = 1$ s with an incidence angle of $\theta_1 = 60°$ along the line $y = 0$ for two different depths. As for normal incidence, the accuracy is only slightly reduced for short times.

Conclusions

In conclusion, we derived a semianalytical solution for the heating of a scattering and absorbing three-layered medium by an incident beam of light, where the light transport is modeled using the P_1 and P_3 approximations to the RTE. We compared our solution to a purely numerical one and observed a good agreement in the case of the P_3 approximation for the light transport. The simpler P_1 approximation showed significantly larger errors and should not be used, given the modest advantage in calculation time compared to the P_3. For the comparison above, the semianalytical solution was several orders of magnitude faster than the numerical solution. An entirely fair comparison is of course difficult to perform, since the numerical simulation unavoidably also yields the absorbance for all positions inside the medium and the temperature for all positions and times. But in most situations, only a small subset of this data is actually required and this is where the semianalytical solution offers large improvements. Finally, some simple generalizations are possible for the heat conduction, since we only require the form of (36). For example, the equation for a moving heat source has the same form with a slightly different α

$$\alpha_u^{(n)} = \sqrt{\frac{\rho^{(n)} c_p^{(n)}}{k^{(n)}} \left(s + iq(u_x \cos\phi_q + u_y \sin\phi_q)\right) + q^2}, \tag{51}$$

where u_x and u_y are the velocity components of the source in the x-y-plane.

A Coefficients $A_2^{(n)}$ and $B_2^{(n)}$ for sources in the second layer

Here, we give closed form expressions for the coefficients $A_2^{(n)}$ and $B_2^{(n)}$ in Eq. (38). The coefficients $A_1^{(n)}$ and $B_1^{(n)}$ are contained in our previous work[26] and $A_3^{(n)}$ and $B_3^{(n)}$ follow immediately by reversing the layer order. Adopting the same notation, the required coefficients follow from the system of equations

$$\begin{pmatrix} (\gamma^{(1)} - \frac{h_1}{k_z^{(1)}})e^{(1)} & -(\gamma^{(1)} + \frac{h_1}{k_z^{(1)}}) & 0 & 0 & 0 & 0 \\ 1 & e^{(1)} & -e^{(2)} & -1 & 0 & 0 \\ k_z^{(1)}\gamma^{(1)} & -k_z^{(1)}\gamma^{(1)}e^{(1)} & -k_z^{(2)}\gamma^{(2)}e^{(2)} & k_z^{(2)}\gamma^{(2)} & 0 & 0 \\ 0 & 0 & 1 & e^{(2)} & -e^{(3)} & -1 \\ 0 & 0 & k_z^{(2)}\gamma^{(2)} & -k_z^{(2)}\gamma^{(2)}e^{(2)} & -k_z^{(3)}\gamma^{(3)}e^{(3)} & k_z^{(3)}\gamma^{(3)} \\ 0 & 0 & 0 & 0 & \gamma^{(3)} + \frac{h_2}{k_z^{(3)}} & -(\gamma^{(3)} - \frac{h_2}{k_z^{(3)}})e^{(3)} \end{pmatrix} \cdot \begin{pmatrix} A_2^{(1)} \\ B_2^{(1)} \\ A_2^{(2)} \\ B_2^{(2)} \\ A_2^{(3)} \\ B_2^{(3)} \end{pmatrix} = \begin{pmatrix} 0 \\ \frac{1}{k_z^{(2)}\gamma^{(2)}} g_1 \\ g_1 \\ -\frac{1}{k_z^{(2)}\gamma^{(2)}} g_2 \\ g_2 \\ 0 \end{pmatrix}, \tag{52}$$

with

$$g_1 = f_2^{(1)}, \tag{53}$$

$$g_2 = f_1^{(2)}. \tag{54}$$

Again using the variables

$$p^{(n)} = 1 + (e^{(n)})^2, \tag{55}$$

$$m^{(n)} = 1 - (e^{(n)})^2, \tag{56}$$

the coefficients are found to be

$$\begin{aligned} A_2^{(1)} = \frac{2}{Mk_z^{(3)}} \left(\frac{h_1}{k_z^{(1)}} + \gamma^{(1)} \right) \Big[& \gamma^{(3)} k_z^{(3)} (g_1 - e^{(2)} g_2)(h_2 p^{(3)} + \gamma^{(3)} k_z^{(3)} m^{(3)}) \\ & + \gamma^{(2)} k_z^{(2)} (g_1 + e^{(2)} g_2)(h_2 m^{(3)} + \gamma^{(3)} k_z^{(3)} p^{(3)}) \Big], \end{aligned} \tag{57}$$

$$\begin{aligned} B_2^{(1)} = \frac{2e^{(1)}}{Mk_z^{(3)}} \left(\gamma^{(1)} - \frac{h_1}{k_z^{(1)}} \right) \Big[& \gamma^{(3)} k_z^{(3)} (g_1 - e^{(2)} g_2)(h_2 p^{(3)} + \gamma^{(3)} k_z^{(3)} m^{(3)}) \\ & + \gamma^{(2)} k_z^{(2)} (g_1 + e^{(2)} g_2)(h_2 m^{(3)} + \gamma^{(3)} k_z^{(3)} p^{(3)}) \Big], \end{aligned} \tag{58}$$

$$\begin{aligned} A_2^{(2)} = \frac{1}{M\gamma^{(2)} k_z^{(1)} k_z^{(2)} k_z^{(3)}} & \Big[-k_z^{(1)} \gamma^{(1)} (g_1 e^{(2)} - g_2)(h_1 p^{(1)} + \gamma^{(1)} k_z^{(1)} m^{(1)}) \\ & + k_z^{(2)} \gamma^{(2)} (g_1 e^{(2)} + g_2)(h_1 m^{(1)} + \gamma^{(1)} k_z^{(1)} p^{(1)}) \Big] \\ & \times \Big[\gamma^{(2)} k_z^{(2)} (h_2 m^{(3)} + \gamma^{(3)} k_z^{(3)} p^{(3)}) - \gamma^{(3)} k_z^{(3)} (h_2 p^{(3)} + \gamma^{(3)} k_z^{(3)} m^{(3)}) \Big], \end{aligned} \tag{59}$$

$$\begin{aligned} B_2^{(2)} = \frac{1}{M\gamma^{(2)} k_z^{(1)} k_z^{(2)} k_z^{(3)}} & \Big[-(\gamma^{(1)})^2 (k_z^{(1)})^2 m^{(1)} + \gamma^{(2)} k_z^{(2)} h_1 m^{(1)} \\ & - \gamma^{(1)} k_z^{(1)} p^{(1)} (h_1 - \gamma^{(2)} k_z^{(2)}) \Big] \times \Big[k_z^{(3)} \gamma^{(3)} (g_1 - e^{(2)} g_2)(h_2 p^{(3)} + \gamma^{(3)} k_z^{(3)} m^{(3)}) \\ & + k_z^{(2)} \gamma^{(2)} (g_1 + e^{(2)} g_2)(h_2 m^{(3)} + \gamma^{(3)} k_z^{(3)} p^{(3)}) \Big], \end{aligned} \tag{60}$$

$$\begin{aligned} A_2^{(3)} = \frac{2e^{(3)}}{k_z^{(1)}} \left(\gamma^{(3)} - \frac{h_2}{k_z^{(3)}} \right) \times \Big[& -\gamma^{(1)} k_z^{(1)} (e^{(2)} g_1 - g_2)(h_1 p^{(1)} + \gamma^{(1)} k_z^{(1)} m^{(1)}) \\ & + \gamma^{(2)} k_z^{(2)} (e^{(2)} g_1 + g_2)(h_1 m^{(1)} + \gamma^{(1)} k_z^{(1)} p^{(1)}) \Big], \end{aligned} \tag{61}$$

$$\begin{aligned} B_2^{(3)} = \frac{2}{k_z^{(1)}} \left(\gamma^{(3)} + \frac{h_2}{k_z^{(3)}} \right) \times \Big[& -\gamma^{(1)} k_z^{(1)} (e^{(2)} g_1 - g_2)(h_1 p^{(1)} + \gamma^{(1)} k_z^{(1)} m^{(1)}) \\ & + \gamma^{(2)} k_z^{(2)} (e^{(2)} g_1 + g_2)(h_1 m^{(1)} + \gamma^{(1)} k_z^{(1)} p^{(1)}) \Big]. \end{aligned} \tag{62}$$

B P_1 solution

For the P_1 approximation, we get only a single eigenvalue

$$\xi_1 = \frac{1}{\sqrt{3\sigma_0\sigma_1}}. \tag{63}$$

The corresponding eigenvector has three components and can be found via the method of rotated reference frames

$$\Lambda_{00}^1 = -\sqrt{3}\sigma_1, \tag{64}$$

$$\Lambda_{10}^{1} = -\sqrt{q^2 + \frac{1}{{\xi_1}^2}}, \tag{65}$$

$$\Lambda_{11}^{1} = -\frac{i}{\sqrt{2}} q. \tag{66}$$

For the particular solution, the system (17) for the P_1 approximation reads

$$\begin{pmatrix} \sigma_0 & -\frac{\mu_c}{\sqrt{3}} & -\sqrt{\frac{2}{3}} iq \\ -\frac{\mu_c}{\sqrt{3}} & \sigma_1 & 0 \\ -\sqrt{\frac{1}{6}} iq & 0 & \sigma_1 \end{pmatrix} \cdot \begin{pmatrix} \chi_{00} \\ \chi_{10} \\ \chi_{11} \end{pmatrix} = \begin{pmatrix} \frac{\mu_s}{\mu_0}(f_0 - f_2)\frac{1}{\sqrt{4\pi}} \\ \mu_s(f_1 - f_2)\frac{3}{\sqrt{4\pi}} \\ \mu_s(f_2 - f_1)\frac{3}{\sqrt{8\pi}}\frac{\sqrt{1-\mu_0^2}}{\mu_0}\cos\phi_q \end{pmatrix}. \tag{67}$$

This system can be solved analytically. Alternatively, the matrix can be LU-decomposed for an efficient numerical solution as

$$\begin{pmatrix} 1 & 0 & 0 \\ 0 & 1 & 0 \\ -\frac{\sqrt{\frac{2}{3}} iq}{\sigma_1} & -\frac{\mu_c}{\sqrt{3}\sigma_1} & 1 \end{pmatrix} \cdot \begin{pmatrix} \sigma_1 & 0 & -\frac{iq}{\sqrt{6}} \\ 0 & \sigma_1 & -\frac{\mu_c}{\sqrt{3}} \\ 0 & 0 & \sigma_0 + \frac{q^2 - \mu_c^2}{3\sigma_1} \end{pmatrix} \cdot \begin{pmatrix} \chi_{11} \\ \chi_{10} \\ \chi_{00} \end{pmatrix} = \begin{pmatrix} \mu_s(f_2 - f_1)\frac{3}{\sqrt{8\pi}}\frac{\sqrt{1-\mu_0^2}}{\mu_0}\cos\phi_q \\ \mu_s(f_1 - f_2)\frac{3}{\sqrt{4\pi}} \\ \frac{\mu_s}{\mu_0}(f_0 - f_2)\frac{1}{\sqrt{4\pi}} \end{pmatrix}. \tag{68}$$

Received: 24 November 2020; Accepted: 18 March 2021
Published online: 19 April 2021

References

1. Abad, B., Borca-Tasciuc, D.-A. & Martin-Gonzalez, M. Non-contact methods for thermal properties measurement. *Renew. Sustain. Energy Rev.* **76**, 1348–1370 (2017).
2. Qu, H., Wang, C., Guo, X. & Mandelis, A. Reconstruction of depth profiles of thermal conductivity of case hardened steels using a three-dimensional photothermal technique. *J. Appl. Phys.* **104**, 113518 (2008).
3. Martínez-Torres, P., Mandelis, A. & Alvarado-Gil, J. J. Optical and thermal depth profile reconstructions of inhomogeneous photopolymerization in dental resins using photothermal waves. *J. Appl. Phys.* **108**, 054902 (2010).
4. Xiao, P., Cowen, J. & Imhof, R. In-vivo transdermal drug diffusion depth profiling-a new approach to opto-thermal signal analysis. *Anal. Sci.* **17icpp**, s349–s352 (2002).
5. Ravi, J. *et al.* Optothermal depth profiling by neural network infrared radiometry signal recognition. *J. Appl. Phys.* **97**, 014701 (2005).
6. Fuente, R., Apiãaniz, E., Mendioroz, A. & Salazar, A. Simultaneous measurement of thermal diffusivity and optical absorption coefficient using photothermal radiometry. i. homogeneous solids. *J. Appl. Phys.* **110**, 033515 (2011).
7. Salazar, A., Fuente, R., Apiãaniz, E., Mendioroz, A. & Celorrio, R. Simultaneous measurement of thermal diffusivity and optical absorption coefficient using photothermal radiometry. ii multilayered solids. *J. Appl. Phys.* **110**, 033516 (2011).
8. Ren, Y., Qi, H., Zhao, F., Ruan, L. & Tan, H. Simultaneous retrieval of temperature-dependent absorption coefficient and conductivity of participating media. *Sci. Rep.* **6**, 21998 (2016).
9. Mármol, G. V. & Villena, J. New 3D in silico model of hair and skin heating during laser hair removal. *Res. J. Pharm. Med. Sci.* **3**, 15–24 (2019).
10. Chandrasekhar, S. *Radiative transfer* (Dover Publications, New York, 1960).
11. Prahl, S. A., Vitkin, I. A., Bruggemann, U., Wilson, B. C. & Anderson, R. R. Determination of optical properties of turbid media using pulsed photothermal radiometry. *Phys. Med. Biol.* **37**, 1203–1217 (1992).
12. Jacques, S. L. & Prahl, S. A. Modeling optical and thermal distributions in tissue during laser irradiation. *Lasers Surg. Med.* **6**, 494–503 (1987).
13. Liemert, A., Reitzle, D. & Kienle, A. Analytical solutions of the radiative transport equation for turbid and fluorescent layered media. *Sci. Rep.* **7**, 3819 (2017).
14. Liemert, A. & Kienle, A. Light transport in three-dimensional semi-infinite scattering media. *J. Opt. Soc. Am. A Opt. Image Sci. Vis.* **29**, 1475–81 (2012).
15. Liemert, A. & Kienle, A. Explicit solutions of the radiative transport equation in the p3 approximation. *Med. Phys.* **41**, 111916 (2014).
16. Wiscombe, W. J. The delta-m method: Rapid yet accurate radiative flux calculations for strongly asymmetric phase functions. *J. Atmos. Sci.* **34**, 1408–1422 (1977).
17. Liemert, A., Martelli, F., Binzoni, T. & Kienle, A. P3 solution for the total steady-state and time-resolved reflectance and transmittance from a turbid slab. *Appl. Opt.* **58**, 4143–4148 (2019).
18. Machida, M., Panasyuk, G. Y., Schotland, J. C. & Markel, V. A. Diffusion approximation revisited. *J. Opt. Soc. Am. A* **26**, 1291–1300 (2009).
19. Markel, V. A. Modified spherical harmonics method for solving the radiative transport equation. *Waves Random Media* **14**, L13–L19 (2004).
20. Panasyuk, G., Schotland, J. C. & Markel, V. A. Radiative transport equation in rotated reference frames. *J. Phys. A: Math. Gen.* **39**, 115–137 (2005).
21. Machida, M., Panasyuk, G. Y., Schotland, J. C. & Markel, V. A. The green's function for the radiative transport equation in the slab geometry. *J. Phys. A: Math. Theor.* **43**, 065402 (2010).
22. Gardner, A. R., Kim, A. D. & Venugopalan, V. Radiative transport produced by oblique illumination of turbid media with collimated beams. *Phys. Rev. E* **87**, 063308 (2013).
23. Williams, M. M. R. The Milne problem with Fresnel reflection. *J. Phys. A: Math. Gen.* **38**, 3841–3856 (2005).
24. Marshak, R. E. Note on the spherical harmonic method as applied to the Milne problem for a sphere. *Phys. Rev.* **71**, 443–446 (1947).
25. Ordonez-Miranda, J., Yang, R., Volz, S. & Alvarado-Gil, J. J. Steady state and modulated heat conduction in layered systems predicted by the analytical solution of the phonon Boltzmann transport equation. *J. Appl. Phys.* **118**, 075103 (2015).

26. Reitzle, D., Geiger, S. & Kienle, A. Semi-analytical solution of the time-dependent heat equation for three-dimensional anisotropic multi-layered media. *Int. J. Heat Mass Transf.* **134**, 984–992 (2019).
27. Bashkatov, A. N., Genina, E. A. & Tuchin, V. V. Optical properties of skin, subcutaneous, and muscle tissues: A review. *J. Innov. Opt. Heal. Sci.* **04**, 9–38 (2011).
28. Duck, F. A. *Physical properties of tissues: A comprehensive reference book* (Academic Press, London, 1990).
29. COMSOL AB. COMSOL Multiphysics v5.2a. www.comsol.com.
30 Reitzle, D. & Geiger, S. rte_heat v1.0, https://doi.org/10.5281/zenodo.4665832 (2021).

Author contributions

D.R. and A.L. derived the solution, D.R. wrote the numerical implementation and prepared the manuscript. S.G. developed the Monte Carlo code and performed the numerical simulations. A.K. supervised the work. All authors reviewed the manuscript.

Competing interests

The authors declare no competing interests.

Additional information

Correspondence and requests for materials should be addressed to D.R.

Reprints and permissions information is available at www.nature.com/reprints.

Publisher's note Springer Nature remains neutral with regard to jurisdictional claims in published maps and institutional affiliations.